2011 50th IEEE Conference on Decision and Control and
European Control Conference (CDC-ECC)
Orlando, FL, USA, December 12-15, 2011

Analysis of a Tunable Impedance Method for Practical Control of Insect-Inspired Flapping-Wing MAVs

Hosein Mahjoubi, and Katie Byl

Abstract—**In the past decade, research into insect-inspired flapping-wing micro-aerial vehicles (FWMAV) has grown steadily, toward addressing unique challenges in morphological construction, force production, and control strategy. Remarkable results have emerged from work focused on generation of adequate lift force for levitation and vertical acceleration [1]; however, effective methods for motion control still remain an open problem. In this paper, we introduce and analyze a novel approach to FWMAV control problem that provides smooth, stable and independent flight in both vertical and horizontal maneuvers. Our insect-inspired MAV model employs a passive structure to adjust the angle of attack (AoA) of its wings. Further analysis of this design unveils its capability in creating significant amounts of net drag force without disturbing lift production. This is the foundation of 'tunable impedance' technique that allows us to independently control three basic motions. One controller regulates yaw and forward acceleration, utilizing intuitive PID control laws in order to control horizontal maneuvers. Lift force and corresponding vertical elevation changes are controlled by a second controller that modifies the frequency of a constant-amplitude, sinusoidal power stroke. A third controller stabilizes the vehicle's body pitch angle through biasing stroke angle of its wings, hence rejecting disturbances caused by fluctuations in the position of center of mass (CoM). Results of simulated experiments confirm that these three controllers together demonstrate exceptional ability in handling hovering or agile flight maneuvers – even in presence of moderate measurement noise. These results also suggest that employment of passive dynamics in the design of MAVs may not only reduce actuator bandwidth requirements – thus simplifying practical implementation of the vehicle – but also improve robustness to uncertainties in sensing and body morphology.**

Keywords—Insect Flight; Microrobotics; Aerial Robotics; Tunable Impedance; Passive Dynamics; Maneuverability; Steering; Simulation.

I. INTRODUCTION

THE modeling, design and control of agile yet robust insect-inspired micro-aerial vehicles (MAVs) remains an ongoing area of research [1]-[4]. Although insects and hummingbirds present inspiring examples of the aerobatics that might eventually be possible in small-scale manmade flyers, it is still unclear how best to simultaneously solve the essential actuation challenges of 1) generating sufficient lift to remain airborne and 2) producing reliable control forces and torques for maneuvering and stabilization of desired motion trajectories. Our work is motivated primarily by the second goal: designing a practical strategy to obtain a complete set of control torques and forces for stable and maneuverable flight. This approach in part parallels the approach of the Wright brothers in focusing on three-axis control of a flight vehicle, controlling both vertical and horizontal motions, as the central problem in obtaining successful aircraft designs. Specifically, the Wright brothers employed "forward canard for pitch/vertical flight path, wing warp for roll and rudder for yaw" [5].

In the present work, we also employ a set of three controllers, toward controlling both horizontal and vertical motions. As in three-axis control for airplanes, two of our controllers for flapping-wing flight act to adjust pitch and yaw angles. Unlike a fixed-wing craft, in which forward velocity must be maintained to produce lift, a flapping-wing vehicle allows for control of vertical thrust that is largely decoupled from forward motion. Our control strategy exploits this feature of flapping-wing flight by including a third controller for vertical height in addition to the controllers for body pitch angle and yaw.

In addition to the importance of having a sufficient set of controllers for maneuverability, we also focus heavily in this work on control solutions that can be implemented in a practical way on small aerial vehicles, i.e., with a wingspan of at most a few centimeters and correspondingly allowing for only minimal payloads to support actuation and sensing requirements. Our approach exploits semi-passive dynamic elements: springs that can be pre-tensioned and for which a set-point can be adjusted over time. Over the past two decades, research in the field of legged robotics has shown that passive dynamics play an essential role in achieving natural-looking and energy-efficient walking gaits [6]-[8]. Similar research in the field of aerial robotics is relatively new. Only a handful of researchers have recently explored the potential of passive principles in achieving appropriate wing motions for effective lift generation [9]-[11].

Although our approach does not mimic true insect flight, it is inspired by a division of control authority that appears to exist in many flying insects [12]. Specifically, many insects employ asynchronous muscles in conjunction with a tuned-mass dynamic system to produce a power stroke at a frequency that cannot be achieved (e.g., greater than 100 Hz) by employing the synchronous muscles humans and other vertebrates use exclusively. Control authority in these agile flyers is achieved not by adjusting the power stroke but instead through the use of more slowly acting flight muscles that tug on the wings throughout the power stroke, to adjust

H. Mahjoubi and K. Byl are with the Robotics Laboratory, Department of Electrical and Computer Engineering, University of California at Santa Barbara, Santa Barbara, CA 93106 USA (e-mail: h.mahjoubi@ece.ucsb.edu, katiebyl@ece.ucsb.edu).

its pitch angle and, correspondingly, adjust the aerodynamic forces generated during flapping [12].

The remainder of the paper proceeds as follows. Section II outlines the approach of tunable impedance upon which this work is based and discusses the options of frequency versus magnitude control of the power stroke in adjusting overall lift. Section III reviews the MAV model used in our simulations, and Section IV describes details each of the three sub-controllers developed and employed. In Section V, we present the results, which indicate very good overall performance in readjusting position and orientation of the vehicle and in recovery from moderate perturbations. Performance in the presence of noise is also investigated, and results show promise for moderate noise but indicate better methods for handling larger levels of noise should be investigated further. Finally, in Section VI, we conclude that our approach provides the desired, largely decoupled motion control that motivates our work. We will also outline future proposed efforts, toward developing this simulated model and control system into a viable, real-world robotic platform.

II. Methodology

The method of tunable impedance is a passive dynamic approach to steering and horizontal motion control of flapping-wing micro-aerial vehicles (FWMAV). As we will soon show, the nature of this method enables us to control horizontal movement of the vehicle without significant interference with its vertical motion. Another feature of this method is its ability to demonstrate fast and smooth performance even when simple PID controllers are used. The presented results in Section V support this claim.

Here, we will first introduce the basic idea behind this method and then incorporate it with a suitable lift control strategy in order to create a complete control law for our FWMAV model.

A. Aerodynamic Force

Our simulations are based on a wing span of $R_w = 15$ mm for a rigid wing shape described in [11]. For a fly-sized MAV, the nominal stroke frequency is about 100 Hz. At this scale, the Reynolds number is low enough (~3,000) to assume that air flow across the wing is quasi-stationary. This allows us to derive a first-order estimate of the produced aerodynamic force F_N [13]–[15] using Blade Element Method [13], [16]. Assuming that the air density is 1.28 kg/m^3, it can be shown [11] that for the wing shape we have chosen, this estimate will be equal to:

$$F_N = 0.2038 \cdot R_W^4 \cdot \sin(\alpha_r) \cdot \dot{\phi} \cdot |\dot{\phi}| \qquad (1)$$

ϕ is the stroke angle of the wing while α_r represents its angle of attack (AoA) relative to local air flow, u_r, as demonstrated in Fig. 1. For simulation purposes, ϕ is always assumed to have a sinusoidal waveform. Since there are no external air currents and the MAV does not reach high velocities, we can replace α_r with $\pi/2$-ψ. Note that ψ is the wing's pitch rotation angle (Fig. 1).

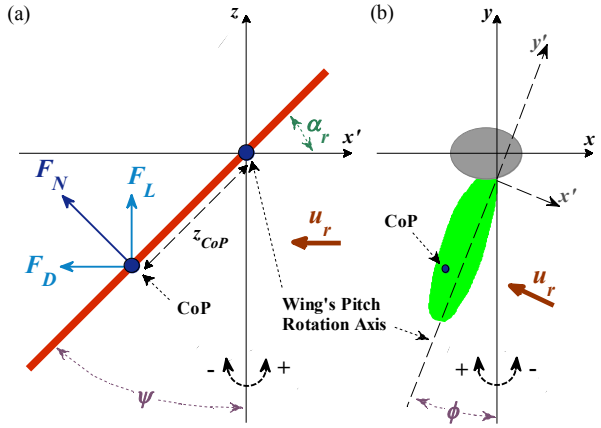

Fig. 1. (a) Wing cross-section (in downstroke) at CoP, illustrating the pitch angle of the wing ψ and orientation of aerodynamic forces. Note that in this case, the produced drag force F_D is negative. (b) Overhead view of the wing/body setup which defines the stroke angle ϕ.

B. Tunable Impedance: Basic Idea

In [11], Byl proposes a mechanical design that passively adjusts the AoA of the wing throughout each stroke, as dictated by its mechanical impedance properties. The torque due to produced aerodynamic force (τ_ψ) balances with a linear torsional spring stiffness, proportional to the wing's pitch rotation angle (τ_k). Assuming that the inertia of the wing is small, this means that the left-hand sides of the following two equations should be equal:

$$\tau_\psi = z_{CoP} \cdot F_N - b_\psi \cdot \dot{\psi} \qquad (2)$$

$$\tau_k = k \cdot (\psi - \psi_0) \qquad (3)$$

Here, z_{CoP} is the distance of center of pressure (CoP) on the wing from the wing's pitch rotation axis (Fig. 1). Passive damping coefficient for wing rotation is shown by b_ψ. The stiffness and set point of the spring are represented by k and ψ_0. From (2) and (3), varying these impedance properties can considerably influence the waveform of ψ, thus causing significant changes in production of aerodynamic force F_N (1). The value of k has a direct impact on the magnitude of aerodynamic force over each stroke cycle. It can be shown that for a sinusoidal stroke waveform ϕ with a fixed magnitude of 35° at 100 Hz, when ψ_0 =0°, the maximum amount of lift force (F_L) is produced when $k = 1.2\times10^{-6}$ N.m/rad. We will use this optimal value for k throughout the rest of this paper.

The relationship between F_N and pitch offset angle ψ_0 is more curious and forms the basis of tunable impedance method. When $\psi_0 = 0°$, the waveforms of ψ and drag force (F_D) during each stroke cycle are odd-symmetric (Fig. 2.a and c). Therefore, if both wings have the same stroke profile, the overall roll and yaw torques will be insignificant. In addition, with zero average drag, forward/backward motion is only possible through changing the pitch angle of the body and thereby, adjusting the projection of F_L on the horizontal plane.

It is possible to achieve nonzero roll/yaw torques by using different stroke profiles for each wing, e.g., different stroke

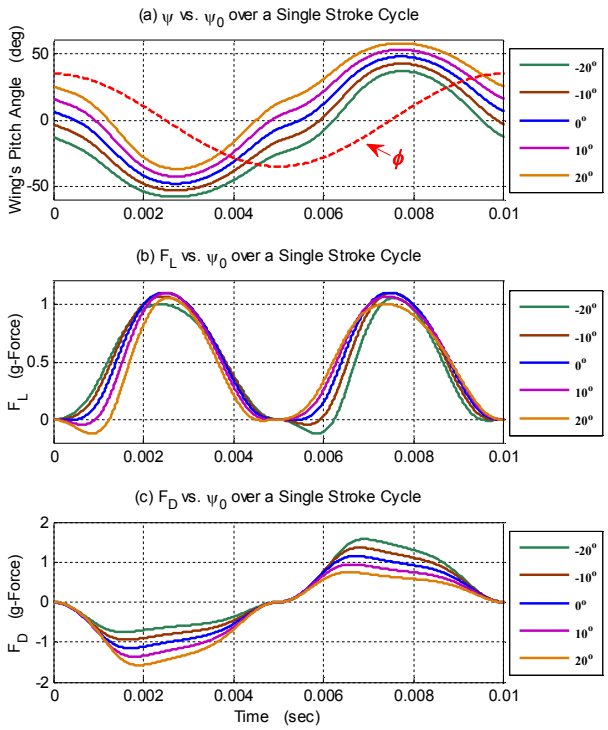

Fig. 2. Evolution of (a) wing's pitch angle ψ, (b) lift force F_L and (c) drag force F_D over a single sinusoidal stroke cycle with a magnitude of 35˚ at 100 Hz. These waveforms are plotted for several values of set point ψ_0 to show the effect of this parameter.

magnitudes or the "split cycle" technique [17]. However, there are two downsides to this approach. First, flapping of each wing has to be done by a separate actuator, causing design challenges due to weight and power constraints. Second, changing the stroke profiles affects both lift and drag forces at the same time. This means that steering/horizontal motion cannot be controlled independently from levitation and we will need a sophisticated motion planning and control strategy to achieve both at the same time.

When solving (1) to (3) for ψ and F_N, the effect of a nonzero ψ_0 can be described as a bias in the waveform of ψ, causing it to become asymmetric (Fig. 2.a). This results in a nonzero average drag force that can be used for forward/backward acceleration or steering (Fig. 3.a). Note that through this approach, both wings can be driven by a single stroke actuator, but they need separate actuators for their corresponding pitch offset angles. However, the bandwidth requirements for these new actuators are low and they can be implemented as structures with little weight [18]. This mechanical feasibility, i.e., trading bigger actuators with smaller ones, is highly desirable since it can greatly help with space and weight constraints.

Fig. 3.a suggests that a change of ±20˚ in the value of ψ_0 can generate significant amounts of average drag force, capable of producing up to 0.25 g's per wing. For the same range in Fig. 3.b, we can see that average lift force is attenuated by less than 10% from its maximum value at ψ_0= 0˚. Correspondingly, controlling the average drag force

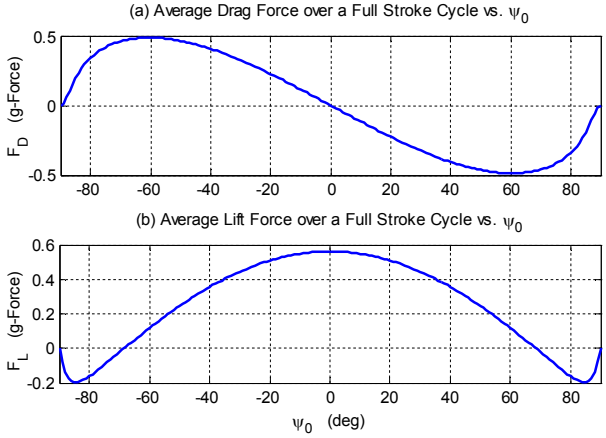

Fig. 3. For a single sinusoidal stroke cycle with a magnitude of 35˚ at 100 Hz, the average aerodynamic force F_N on one wing is calculated as the wing's pitch offset angle ψ_0 is changed. For small values of ψ_0, (a) the magnitude of drag component increases significantly, while (b) the magnitude of lift component only slightly decreases.

through changing ψ_0 in a limited range does not affect the average lift force significantly. This allows us to control vertical and horizontal maneuvers independently, as confirmed by our simulation results in Section V.

C. Lift Control

Assuming that the stroke angle of the wing is a sinusoidal function of time, i.e. $\phi = A\cos(\omega t)$, from (1) it can be seen that the average aerodynamic force during each flapping cycle is an almost quadratic function of both stroke magnitude A and the stroke frequency ω. Fig. 4 confirms similar relationships between the average lift force and aforementioned parameters.

The muscle structure of many insects suggests that in order to adjust lift force, they can employ both strategies of changing their stroke magnitude and/or frequency of flapping [19]. Although controlling stroke magnitude can provide good theoretical performance [20], we anticipate that a constant-magnitude stroke motion with variable frequency may be much more practical to implement, e.g.,

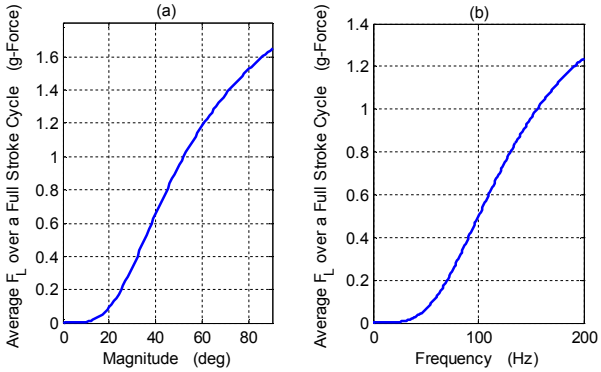

Fig. 4. In a set of simulated experiments, the effect of stroke profile parameters on average lift force of a single wing was investigated. (a) In the first group, frequency was set to 100 Hz and the average lift force over one stroke cycle was calculated for various stroke magnitudes. (b) In the second group, stroke magnitude had a fixed value of 35˚ and the average F_L was calculated for various values of stroke frequency. In both groups, ψ_0 was always 0˚.

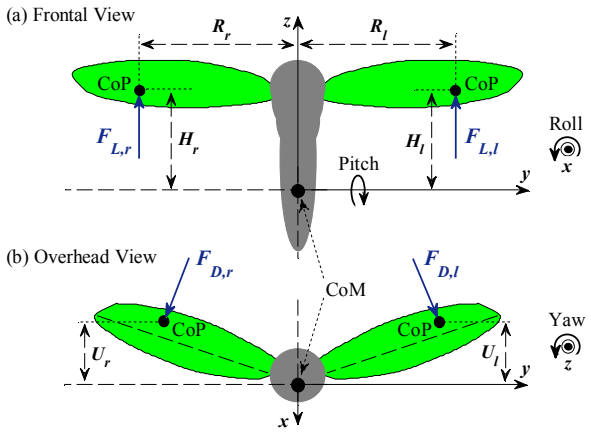

Fig. 5. Free-body diagram of a FWMAV: (a) frontal and (b) overhead view. R, H and U specify the location of center of pressure (CoP) of each wing with respect to the center of mass (CoM) of the whole system. Indices l and r represent left and right, respectively.

by using a reciprocating mechanical linkage. Of course, this choice calls for high-bandwidth actuators, e.g. piezoelectric bimorphs. As for performance, we will compare the takeoff/hovering responses of both methods in Section V.A to investigate them in terms of speed and stability of flight. These results also encourage us to choose frequency adjustment as our approach for lift control.

III. Modeling

Fig. 5 illustrates a free-body diagram of a typical FWMAV. By applying Newton's equations of motion in this body frame, a complete dynamic model of the MAV is developed [2] that will be used in all of our simulated experiments. For simulation purposes, Euler angles in the Tait-Bryan ZXY convention are used to define and update the body angles.

It is assumed that passive damping while rotating around either axis can be accurately modeled as a linear function of corresponding angular velocity [21]. In addition, viscous friction along each axis is modeled as a quadratic function of linear velocity along that axis. Physical properties of the model and their values are listed in Table I.

TABLE I
PHYSICAL PROPERTIES OF THE MODELED FWMAV

Symbol	Description	Value
m_{body}	total mass	7×10^{-5} kg
J_{body}	inertia matrix (a 3×3 scalar matrix)	3×10^{-8} N.m.s^2
R_w	length of wing chord	1.5×10^{-2} m
z_{CoP}	distance of CoP of each wing from its pitch rotation axis	1.009×10^{-3} m
b_ψ	passive damping coefficient of the wings (pitch rotation)	5×10^{-10} N.m.s
b_ω	passive damping coefficient of the body (rotation in either direction)	3×10^{-6} N.m.s
b_v	coefficient of viscous friction along either direction	1×10^{-4} N.s^2/m^2
$H(\psi=0^\circ)$	distance of CoP from transverse plane of the body (xy) when $\psi=0^\circ$	5.42×10^{-3} m
$R(\phi=0^\circ)$	distance of CoP from sagittal plane of the body (xz) when $\phi=0^\circ$	1.191×10^{-2} m
W_{body}	body width at the root of wings	2.16×10^{-3} m
$U(\phi=0^\circ)$	distance of CoP from coronal plane of the body (yz) when $\phi=0^\circ$	1.08×10^{-3} m

From Fig. 5, note that we deliberately consider the more challenging but realistic case in which center of mass (CoM) is not directly below the overall center of lift (CoL) of the vehicle, i.e., U_r and U_l (see Fig. 5) have nonzero average values. Remember that up to this point, ϕ was assumed to be a sinusoid with an average value of 0°. In a situation like this, the lift force considerably increases the amount of pitch torque, making it more difficult to stabilize the MAV. To address this issue, the stroke angle of both wings can be biased appropriately in order to push CoL above CoM, hence minimizing the pitch torque induced by lift force. Biasing is controlled based on pitch angle of the MAV. The details of this process are discussed in the next section.

IV. Controller

A control structure based on ideas introduced in Section II has been developed. Fig. 6 illustrates a block diagram of this design. As it can be seen, there are three main modules that are responsible for control of pitch angle, altitude and horizontal maneuvers. All these blocks are simulated in discrete-time with a variable time step, i.e. they update their output once per stroke cycle.

Before discussing the details of each sub-controller, note how their outputs are used to produce actual outputs of the controller. In each stroke cycle, the sine wave generator creates a reference stroke waveform with a fixed magnitude of 35° based on values of stroke frequency and bias angle. This magnitude is chosen to ensure production of sufficient lift force for levitation at a nominal stroke frequency of 100 Hz (see Fig. 3.b and 4.a). To have a more realistic estimate of the stroke profile, this reference waveform is then fed to a low-pass filter to model the piezo-actuator (Fig. 6). The resulting output along with values of ψ_0 are then used in calculation of aerodynamic forces and wings' pitch rotation angles throughout the stroke cycle.

A. Altitude Controller

In Section II, we investigated the relationship between

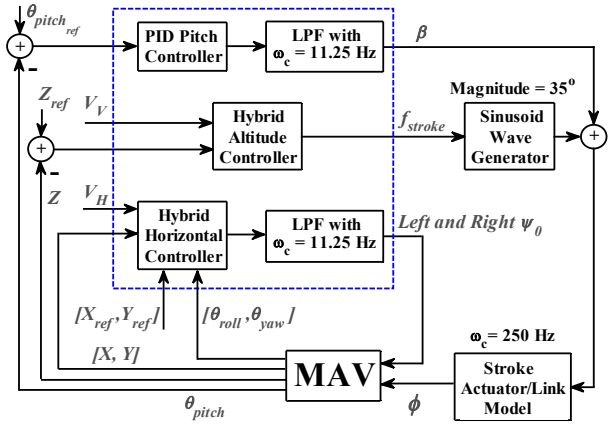

Fig. 6. Block diagram of the modeled MAV's controller system. In each stroke cycle, the sinusoid wave generator creates a reference stroke waveform with a fixed magnitude of 35° based on calculated values for stroke frequency and bias angle β. Crossover frequency of each filter/actuator is represented by ω_c.

stroke frequency and average lift force. We can use this to control the altitude of the MAV by appropriately adjusting its frequency of flapping. This is done using a hybrid controller (Fig. 6). Whenever a change in altitude is required, a proportional controller is activated to stabilize the average vertical velocity at the reference value of $V_V = 1$ m/s. Upon reaching the vicinity of the desired height, command is switched to a PID controller that stabilizes the vehicle's vertical position at the target altitude.

Before sending the output frequency to the sine wave generator, it is limited between 50 and 200 Hz. The upper saturation limit is to account for bandwidth limitations of the actuator. We also chose a minimum value of 50 Hz to ensure that when lift force is decreased, e.g., when losing altitude, the drag force remains large enough for any possible horizontal maneuver.

B. Pitch Controller

As discussed earlier, with no bias added to the waveform of the stroke angle, the CoM of our model is not exactly below the average location of the overall CoL. Changing the bias angle allows us to move the average location of CoL, thereby adjusting the induced pitch torque due to lift force. This can be used to control and stabilize the pitch angle of MAV. Note that adding a bias does not influence the angular velocity of stroke and therefore, does not change the lift force itself.

A PID controller is in charge of stabilizing pitch angle at the target value. Target pitch angle may vary depending on the required maneuver, but in our simulations, we never had to use a commanded pitch value larger than 4˚ in magnitude. The calculated bias angle is then limited to ±15˚ (Fig. 6) to ensure that the stroke angle remains between -50˚ and 50˚.

C. Steering/Horizontal Motion Controller

Whenever the altitude controller changes the stroke frequency, both lift and drag forces are affected. However, the tunable impedance method enables the model to generate sufficient average drag force for horizontal maneuvers in spite of frequency variations. This is done by applying small changes in each wing's pitch offset angle ψ_0, which, as observed in Fig. 3.b, do not cause significant alteration in the average lift. To remain in this operating zone (Fig. 3.b), the outputs of the horizontal controller (Fig. 6) are saturated at ±25˚ prior to being sent to the next stage.

Pitch offset angles are adjusted by a hybrid controller. In the first stage, the deviation angle of the MAV's current heading from the target is calculated. If the magnitude of this variable is larger than 2˚ and smaller than 175˚, the steering controller is activated. The magnitudes of both wings' pitch offset angles are then set to an equal value proportional to the deviation angle from target. Finally, the sign of each wing's ψ_0 is set according to the required direction of yaw. For instance, when turning left, the right and left hand wings should have negative and positive pitch offset angles, respectively (see the results in Section V.*C*).

Once the deviation angle is sufficiently small, a module with the same structure as the altitude controller is activated to control the forward/backward motion of the MAV. Here, the reference value for horizontal velocity is also set to V_H = 1 m/s throughout all simulations. Note that in this mode, the same value is assigned to pitch offset angles of both wings.

Nonzero pitch offset angles create a net drag force on each wing, which in turn generates both yaw and roll torques. The MAV uses these yaw torques for steering, but roll torques disturb the balance of the vehicle. To negate the induced changes in roll angle, we can create a small imbalance between lift forces of each wing. First, based on the magnitude of roll angle (θ_{roll}), a new coefficient γ is calculated:

$$\gamma = \max(0,\ \ 1 - \eta \cdot |\theta_{roll}|) \tag{4}$$

where $\eta = 100$ is a positive constant gain. Note that if roll angle is small, γ stays close to 1, but when it becomes large, γ will be set to 0. The calculated ψ_0 for the side of the vehicle that has rolled downward will then be attenuated by a factor of γ. This will slightly increase the net lift force on that side (Fig. 3.b), creating a roll torque that tends to decrease the magnitude of MAV's roll angle.

V. Simulation Results

Through a set of preliminary tuning experiments, reasonable values were chosen for gains and time constants of the controller described in Section IV. The tuned sub-controllers are listed in Table II. In this section, we present and discuss simulation results for a variety of maneuvers to evaluate flight performance of the MAV when navigated by the proposed controller.

A. Takeoff and Hovering

In Section II, we indicated that lift force can be controlled by adjusting either 1) frequency or 2) magnitude of stroke. The described controller in Section IV is based on the first approach. There are two main reasons for our choice, the first being simplicity of implementation.

The second reason is the slightly more stable flight observed when using this kind of control. To show this, a simulated experiment was arranged where the hovering MAV is commanded to first raise its altitude by 1 m and then reenter hovering state (Fig. 7.a-d). In a similar experiment (Fig. 7.e-h), the altitude controller was modified to adjust the magnitude of stroke instead of its frequency – now fixed at 100 Hz. The gains of this new controller were set so that its resulting altitude response (Fig. 7.e) stays close

TABLE II
TUNED SUB-CONTROLLERS

Transfer Function	Description
25	proportional vertical velocity controller
50+1/s+5s	PID vertical position controller
10+2/s+0.05s	PID pitch controller
200	proportional yaw controllers
25	proportional horizontal velocity controllers
2000+1/s+100s	PID horizontal position controllers

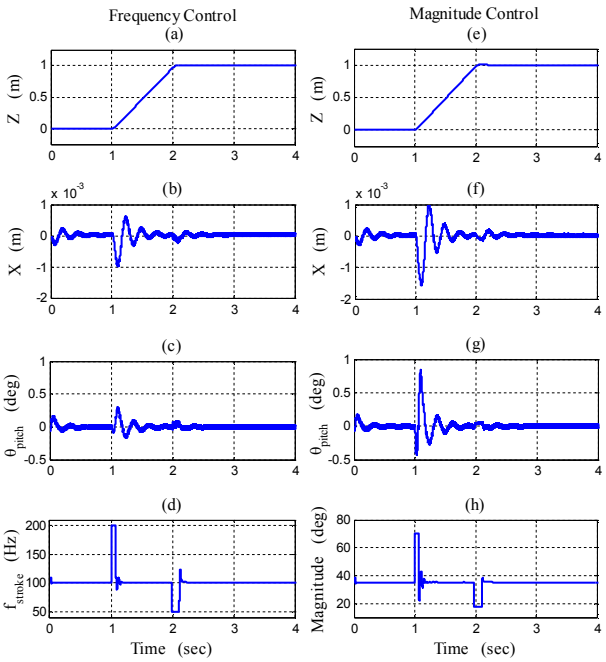

Fig. 7. Evolution of altitude Z, sagittal displacement X, pitch angle and altitude control variable in a simulated takeoff/hovering experiment: (a)-(d) when adjusting stroke frequency and (e)-(h) when adjusting stroke magnitude to control lift force. In both cases, roll and yaw angles of the MAV remain close to 0˚. Coronal displacement Y is also very small and is not displayed.

to that of the first experiment (Fig. 7.a), i.e. the MAV is stabilized at the new altitude by $t = 2$ seconds. In both cases, lift control parameter is always quickly stabilized at its nominal value (Fig. 7.d and 7.h). However, it seems that in the second experiment, the produced aerodynamic force experiences larger fluctuations. As a result, horizontal position and pitch angle of the MAV are slightly less stable (Fig. 7.f and 7.g in comparison to Fig. 7.b and 7.c).

In the remainder of this paper, lift force is always controlled through adjustment of stroke frequency.

B. Pitch Tracking

To examine the performance of pitch control, the MAV's response to a sequence of reference pitch angle values was simulated (Fig. 8.c). With each change in the reference pitch angle, the controller adjusts the amount of stroke angle bias accordingly as discussed in Section IV.*B* (Fig. 8.d) to track the given reference. From Fig. 8.c, the MAV is capable of reaching all desired pitch angles at a rate of either 30˚/sec or -15˚/sec depending on whether it is pitching forward or backward, respectively.

The model is initially in hovering mode. Whenever pitch angle is altered, vertical and horizontal components of aerodynamic force change, too. This will cause motion in both directions. However, the altitude and horizontal motion controllers act to keep the MAV at the origin, i.e. at the reference position of hovering. Fig. 8.a and 8.b illustrate that the MAV does slightly move in both directions, but in each case, the motion is stabilized in a location near the origin. Note that the set points are changed at a low pace (Fig. 8.f).

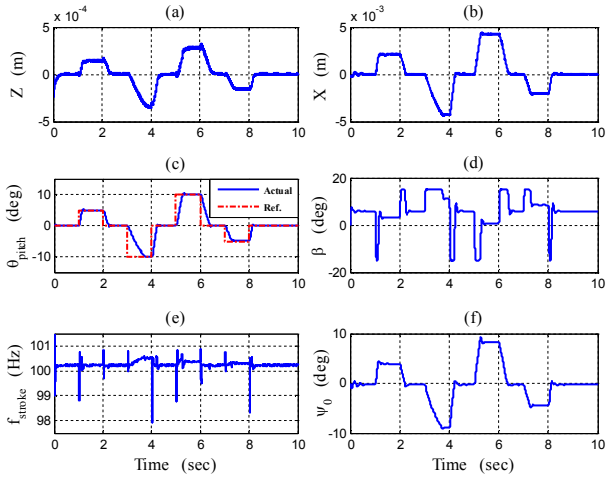

Fig. 8. Pitch angle tracking in hovering mode: evolution of (a) altitude Z, (b) sagittal displacement X, (c) pitch angle, (d) stroke bias angle β, (e) frequency of stroke and (f) pitch offset angle ψ_0 of either wing. Both roll and yaw angles of the MAV remain close to 0˚. Coronal displacement Y is also very small and is not displayed.

C. Steering and Horizontal Motion

In the most general group of experiments, the modeled MAV was expected to reach a specified target position $[X_{ref}, Y_{ref}, Z_{ref}]$, starting from hovering condition. The target was always placed in a location where accessing it required both steering and forward/backward motion. In some cases, target and MAV also had an initial altitude difference in order to investigate whether horizontal motion control interferes with performance of altitude controller. Fig. 9 illustrates one such experiment.

At $t = 1$ seconds, target position is switched from origin to (1 m, 1 m, 1 m). It takes the MAV about 0.9 seconds to

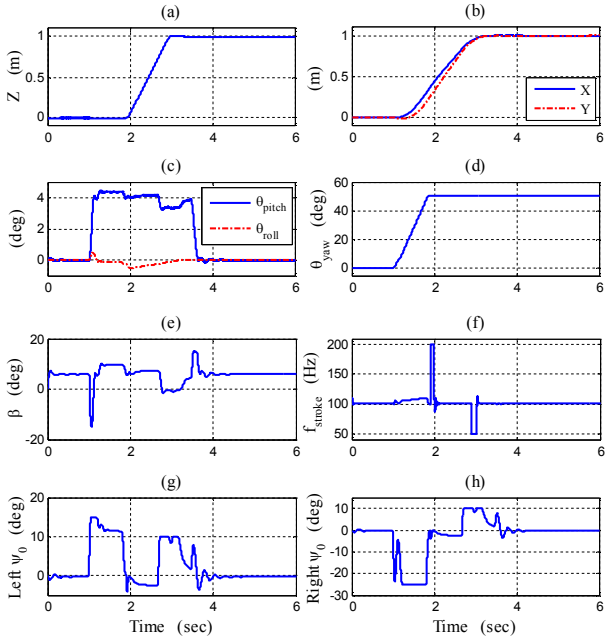

Fig. 9. A simulated multi-maneuver experiment: evolution of (a) altitude Z, (b) X and Y coordinates of position, (c) pitch, roll and (d) yaw angles of the body, (e) stroke bias angle β, (f) frequency of stroke, (g) pitch offset angle ψ_0 of left and (h) right hand wings.

reorient and start moving towards the target (Fig. 9.d). New altitude is reached and stabilized within the next second (Fig. 9.a). For the same thing to happen in horizontal plane, 1.5 seconds is required (Fig. 9. b). This means that overall maneuver is completed in 2.4 seconds and after that, the MAV continues to hover at the new location.

Fig. 9 confirms that with the proposed controller in Section IV, the MAV model is able to perform various maneuvers in a both stable and considerably fast manner. A comparison between Fig. 7.a and Fig. 9.a suggests that adjustment of ψ_0 by the horizontal motion controller does not affect lift control significantly. Therefore, we can safely assume that vertical and horizontal maneuvers are performed almost independently. Finally, note that Fig. 9.g and 9.h illustrate the evolution of pitch offset angles of the left and right hand wings, respectively. As it can be seen, these parameters do not change at a very high rate. This supports our notion that pitch offset angle actuators have low bandwidth requirements.

D. Perturbation Recovery

Various impact and perturbation scenarios were simulated to investigate the capability of controller in returning the MAV to a stable state. The example in Fig. 10 shows a case where a large external force briefly hits the hovering MAV from right-front direction at $t = 1$ seconds, modeled as an instantaneous disorientation in pitch, roll and yaw angles of the vehicle (Fig. 10.c-d). The impact also provides an initial velocity which causes the MAV to move away from the origin (Fig. 10.a-b).

Shortly after the impact, controller begins to stabilize the model by minimizing roll angle and turning the vehicle towards its original position. Once the orientation is recovered, the MAV moves to the target and resumes its hovering. The whole process takes less than 2.4 seconds. Hence, in terms of perturbation recovery, the proposed controller is both reliable and relatively fast.

E. Performance in Presence of Noise

All the experiments described so far were simulated in the absence of noise. To investigate the performance of our control approach in presence of noise, we repeated the experiments of part *C*, this time adding white measurement noise to all feedback parameters. Various levels of noise magnitude were applied. The results suggest that our current controller cannot handle large amounts of noise effectively and may fail to stabilize the MAV. We believe that our choices of PID control law along with low switching thresholds are the main reasons for this shortcoming. A more sophisticated controller is expected to improve navigation performance in presence of significant amounts of noise.

Fig. 11 shows a case in which measurement noise has a small magnitude. This is the same experiment as the one in Fig. 9, repeated with Gaussian white noise added to feedback position and orientation. The noise on each "measured" component of position has a standard deviation of 2.5 mm. The noise on each "measured" angle has a standard deviation of 0.5°. As before, "measurement" and sampling is done once per stroke cycle.

The MAV still manages to reach the target and enter hovering state in a slightly larger time interval. But compared to the noise-free case, performance has degraded. This degradation specifically demonstrates itself in evolution of body angles (Fig. 11.c-d). In addition, the sensor noise

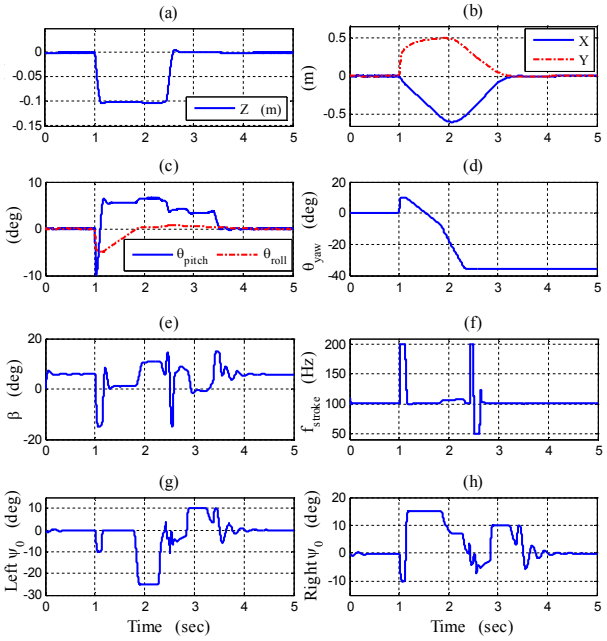

Fig. 10. Hovering MAV's recovery from a perturbation applied at t =1 seconds: evolution of (a) altitude *Z*, (b) *X* and *Y* coordinates of position, (c) pitch, roll and (d) yaw angles of the body, (e) stroke bias angle β, (f) frequency of stroke, (g) pitch offset angle ψ_0 of left and (h) right hand wings.

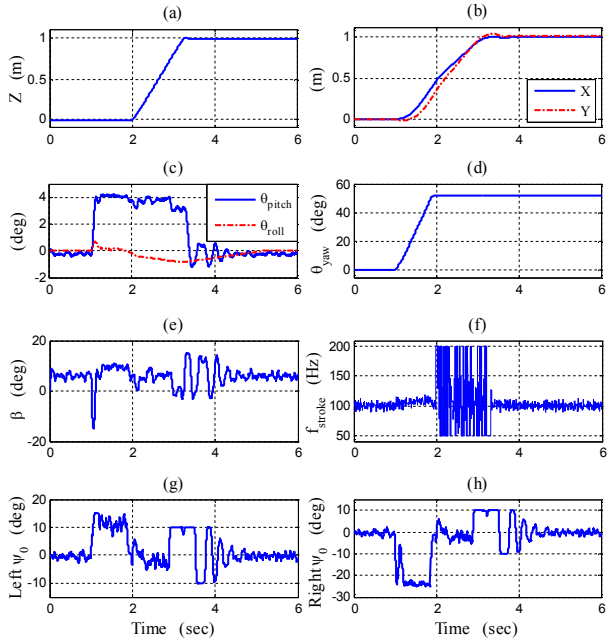

Fig. 11. A simulated multi-maneuver experiment when a small amount of white measurement noise is present: evolution of (a) altitude *Z*, (b) *X* and *Y* coordinates of position, (c) pitch, roll and (d) yaw angles of the body, (e) stroke bias angle β, (f) frequency of stroke, (g) pitch offset angle ψ_0 of left and (h) right hand wings.

causes larger position fluctuations during hovering. However, the overall performance of the controller is still acceptable and can be considered relatively fast.

Note that process noise with low magnitude can be used to model small physical differences between the left and right sides of an actual MAV's body. It can also represent small undesired differences between impedance actuators of both sides. Therefore, we expect that in a real system, our controller can deal with such imperfections.

VI. Conclusion and Future Work

In essence, tunable impedance is a passive-based approach to control the drag forces on a FWMAV, thereby navigating the vehicle for horizontal in-plane motion. Here, pitch rotation of each wing throughout every stroke cycle is governed by a passive structure, i.e., a torsional spring. The idea is to create asymmetries in the stroke profile of both wings by adjusting their impedance properties, thus changing the amount of net drag force produced by each wing. Depending on the direction of these forces, vehicle can move forward/backward or reorient in a new direction.

Small variations in a wing's pitch offset angle can produce a considerable amount of drag with insignificant interference in production of lift. This feature of tunable impedance technique allows the MAV to perform horizontal and vertical maneuvers almost independently. However, the need for impedance adjustment in each wing has the downside of adding two more actuators to the final design. Fortunately, these can be low-powered actuators with low bandwidth requirements and should not considerably complicate the design problem.

The performance of the proposed control system (Fig. 6) was examined in various simulated situations. In all cases, the modeled MAV demonstrated both agile and smooth transition between two locations and always managed to enter hovering state within a very small distance from the target. A stroke bias sub-controller enables the vehicle to compensate imbalances in the position of CoM and to reach body pitch angles required for these maneuvers without destabilization. Results of simulated experiments in the presence of disturbances and small amounts of measurement noise show that our control approach is quite capable of perturbation recovery and can handle disturbances created by small imperfections such as physical differences or actuation asymmetries between the left and right sides of the vehicle.

While our current PID controllers can only handle moderate amounts of noise effectively, they clearly show the potential of our general approach in employment of simple control laws. Modification of these controllers to reduce the effects of noise is part of the agenda for our future work. We note that our model does not account for the effects of wing inertia. While this simplification is reasonable for an insect-sized aircraft, it may become inappropriate as the scale of an MAV increases. Therefore, this is another issue that will be addressed in our future work. We intend to implement the final results on a 3-inch-wingspan MAV. We also plan to merge our motion control approach with a suitable path planning and navigation algorithm in order to test the vehicle in field experiments.

References

[1] R. J. Wood, "The first takeoff of a biologically inspired at-scale robotic insect," *IEEE Transactions on Robotics*, 24, pp. 341–347, 2008.

[2] X. Deng, L. Schenato, W. C. Wu, and S. S. Sastry, "Flapping flight for biomimetic robotic insects: part I–system modeling," *IEEE Transactions on Robotics*, 22(4), pp. 776–788, 2006.

[3] X. Deng, L. Schenato, W. and S. S. Sastry, "Flapping flight for biomimetic robotic insects: part I–flight control design," *IEEE Transactions on Robotics*, 22(4), 780–803, 2006.

[4] M. Hamamoto, Y. Ohata, K. Hara, and T. Hisada, "A fundamental study of wing actuation for a 6-in-wingspan flapping microaerial vehicle," *IEEE Transactions on Robotics*, 26(2), pp. 244–255, 2010.

[5] G. D. Padfield, and B. Lawrence, "The birth of flight control: an engineering analysis of the Wright brothers' 1902 glider," *The Aeronautical Journal of the Royal Aeronautical Society*, 107(1078), pp.697–718, 2003.

[6] T. McGeer. "Passive dynamic walking," *The International Journal of Robotics Research*, 9(2), pp. 62–82, 1990.

[7] A. Goswami, B. Espiau, and A. Keramane, "Limit cycles and their stability in a passive bipedal gait," Proceedings of IEEE International Conference on Robotics and Automation *(ICRA)*, pp. 246–251, 1996.

[8] S. H. Collins, A. Ruina, R. Tedrake and M. Wisse, "Efficient bipedal robots based on passive-dynamic walkers," *Science*, 307, pp. 1082–1085, 2005.

[9] A. J. Bergou, S. Xu and Z. J. Wang, "Passive wing pitch reversal in insect flight". J. Fluid Mech., 591, pp. 321–337, 2007.

[10] P. S. Sreetharan, and R. J. Wood, "Passive torque regulation in an underactuated flapping wing robotic insect," Robotics: Science and Systems, Zaragoza, Spain, June 2010.

[11] K. Byl, "A passive dynamic approach for flapping-wing micro-aerial vehicle control," 2010 ASME Dynamic Systems and Control Conf., Cambridge, MA, USA, September 13-15, 2010.

[12] R. Dudley, *The Biomechanics of Insect Flight: Form, Function, Evolution*. Princeton University Press, 2000.

[13] C. P. Ellington, "The aerodynamic of hovering insect flight I. the quasi-steady analysis," *Philosophical Transactions of the Royal Society of London*, 305(1122), pp. 1–15, 1984.

[14] S. P, Sane, and M. H. Dickinson, "The control of flight by a flapping wing: lift and drag production," *Journal of Experimental Biology*, 204, pp. 2607–2626, 2001.

[15] W. B. Dickson, and M. H. Dickinson, "The effect of advance ratio on the aerodynamics of revolving wings," *Journal of Experimental Biology*, 207, pp. 4269–4281, 2004.

[16] M. F. M. Osborne, "Aerodynamics of flapping flight with application to insects," *Journal of Experimental Biology*, 28(2), pp. 221–245, 1951.

[17] D. B. Doman, and M. W. Oppenheimer, "Dynamics and control of a minimally actuated biomimetic vehicle: part I. aerodynamic model," 2009 AIAA Guidance, Navigation, and Control Conf., San Francisco, CA, USA, August 10-13, 2009.

[18] T. Miura, T. Shirai, and T. Tomioka, "Proposal of joint stiffness adjustment mechanism SAT," JSME Conference on Robotics and Mechatronics '02, pp. 29, 2002. (in Japanese)

[19] R. K. Josephson, "Chapter 3: Comparative Physiology of Insect Flight Muscle," in *Nature's versatile Engine: Insect Flight Muscle Inside and Out*. (Vigoreaux and Josephson, ed.) pp. 34–43, Springer USA, 2006.

[20] N. O. Perez-Arancibia, J. P. Whitney, and R. J. Wood, "Lift force control of flapping-wing microrobots," to appear: *IEEE transactions on Mechatronics*, 2011.

[21] T. L. Hedrick, B. Cheng, and X. Deng, "Wingbeat time and the scaling of passive rotational damping in flapping flight," *Science*, 324(5924), pp. 252–255, 2009.